Electronic Supplementary Material

Abnormal Linear Dichroism Transition in Two-Dimensional PdPS

Gang Li,[3,†] Zheng Chen,[2,†] Hanlin Zhang,[3] Mengxi Yu,[3] Hui Zhang,[3] Jiawnag Chen,[1] Zihan Wang,[3] Shiqi Yin,[3] Weichang Lin,[4] Penglai Gong,[5,*] Longhui Zeng,[6] Xiangde Zhu,[2] Wensen Wei,[2] Mingliang Tian,[2,*] and Liang Li,[1,3] *

[1]Key Laboratory of Materials Physics, Anhui Key Laboratory of Nanomaterials and Nanotechnology, Institute of Solid State Physics, Hefei Institutes of Physical Science, Chinese Academy of Sciences, Hefei 230031, P.R. China, University of Science and Technology of China, Hefei 230026, P.R. China

[2]High Magnetic Field Laboratory, Chinese Academy of Science, Hefei 230031, P. R. China

[3]Institutes of Physical Science and Information Technology, Anhui University, Hefei 230601, P. R. China

[4]Applied Physics and Applied Mathematics Department, Fu Foundation School of Engineering and Applied Science, Columbia University, New York, NY 10027, USA

[5]Key Laboratory of Optic-Electronic Information and Materials of Hebei Province, Institute of Life Science and Green Development, College of Physics Science and Technology, Hebei University, Baoding 071002, China

[6]Department of Applied Physics, The Hong Kong Polytechnic University, Kowloon, Hong Kong, China

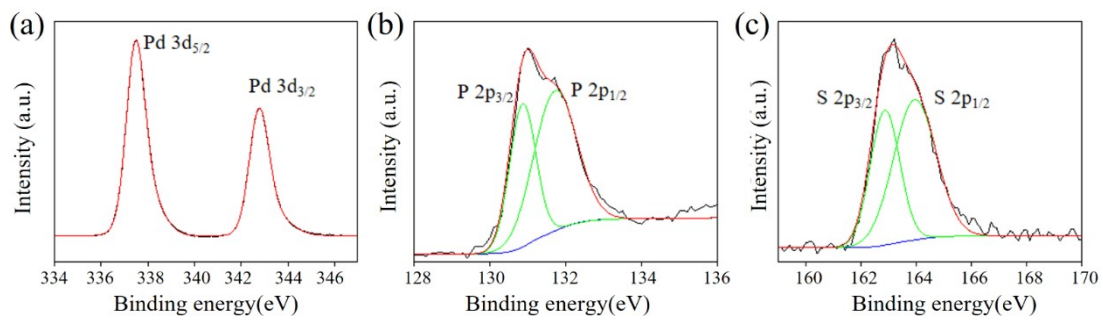*Corresponding author (E-mail: gongpl@hbu.edu.cn; tianml@hmfl.ac.cn; liliang@issp.ac.cn)

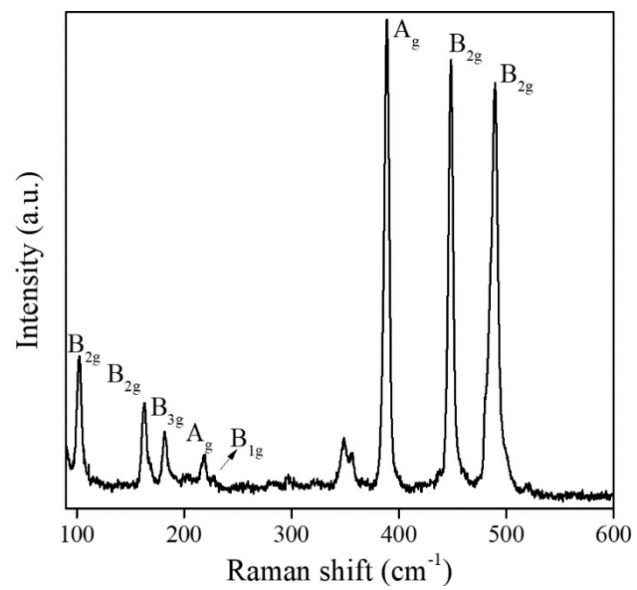**Fig S1.** XPS spectra of Pd_{3d}, P_{2p} and S_{2p} core level.

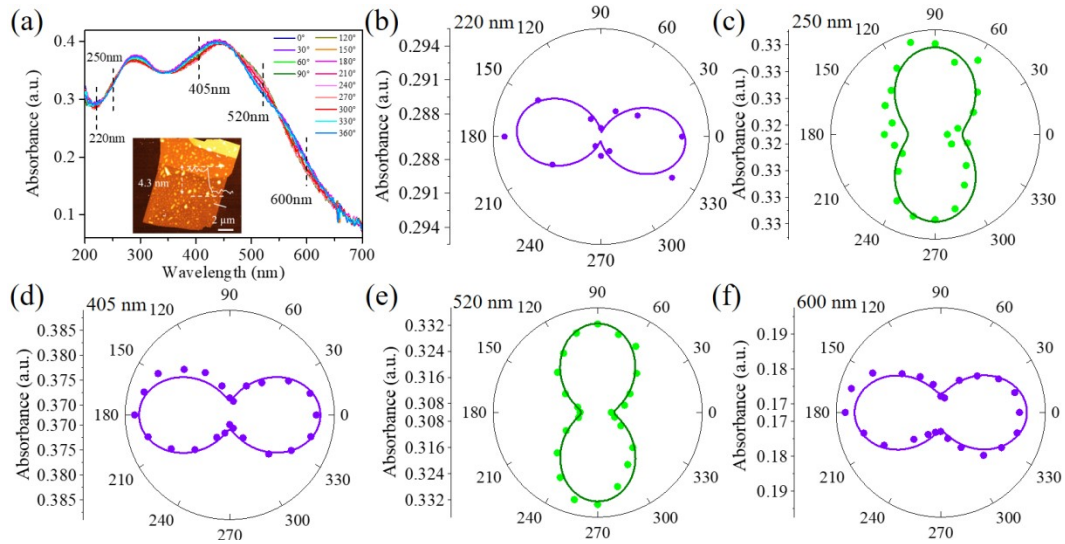**Fig S2.** The Raman spectrum of PdPS flake.

Fig S3. The polarization-sensitive absorption of PdPS flake. (a) Polarization-resolved absorption spectra of 4.3 nm PdPS within the spectral range of 200−700 nm. The inset AFM image of the sample is shown in the lower-left corner. Polar plot and fitting of (b) 220 nm, (c) 250 nm, (d) 405 nm, (e) 520 nm, (f) 600 nm.
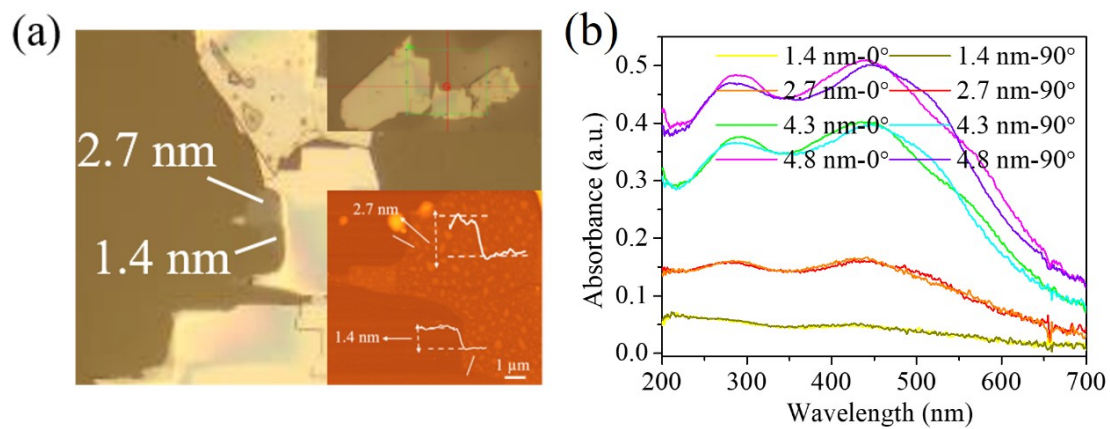
Fig S4. (a) Typical OM image and AFM image (inset) of exfoliated PdPS flake. (b) Polarization-resolved absorption spectra of PdPS within the spectral range of 200−700 nm.
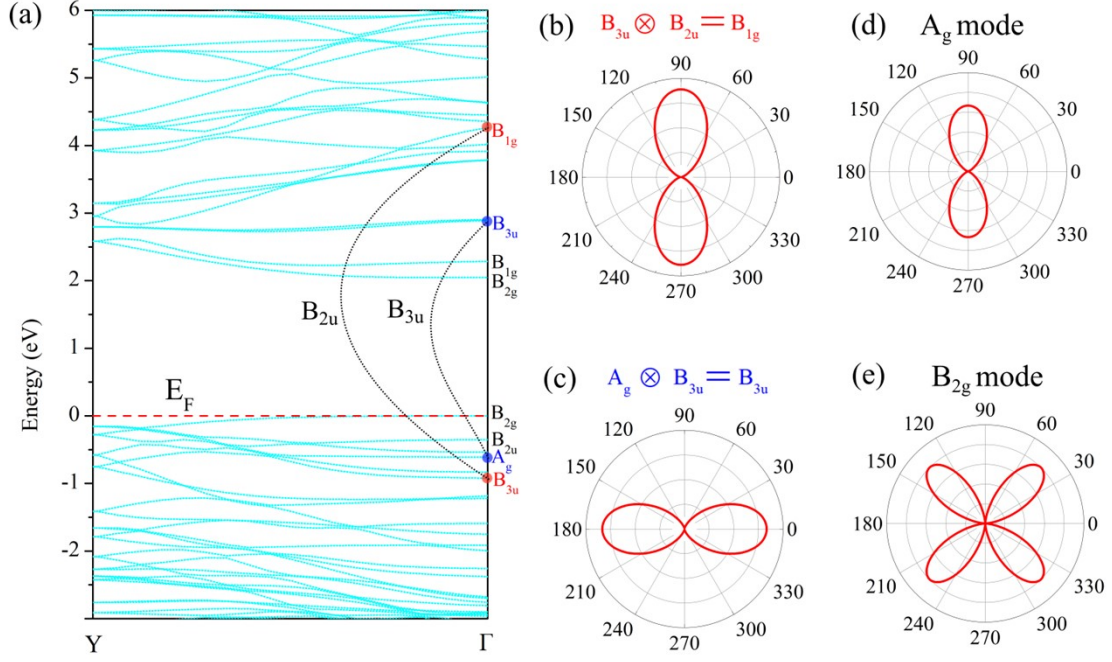
Fig S5. Calculated polarization dependence of the absorption intensity and the Raman intensity in bulk PdPS for two optical transitions allowed by symmetry. (a) Band structure of bulk PdPS along the Γ-Y direction. Irreducible representations of selected energy bands near the Fermi level (E_F) at the Γ point are shown. (b) and (c) Two different possible optical transitions in bulk PdPS with the corresponding symmetry restrictions. (d) and (e) Schematic diagram for the Raman intensity of the A_g mode and the B_{2g} mode.

The "selection rules" was used to understand the linear dichroism transition in the optical transition and Raman spectra. All the irreducible representations of bulk PdPS at the Γ point was calculated, some of which near the Fermi level are shown in Figure S5a. Because PdPS and GeAs$_2$ have the same character table for the D_{2h} point group at the Γ point (Table S1), they follow the same selection rules in the optical transition and Raman spectra [1]. Hence we focus on explaining the secelected transitions. More details about the slection rules can be found in the "Note S2: Seclection rules" in the Supporting Information of our previous work[1].

In view of the character table of D_{2h}, two possible irreducible representations for light polarizations are shown in the Table S1, namely, B_{3u} for the x-polarized light and B_{2u} for the y-polarized light. When the symmetry of the initial state $|i\rangle$ provided, we can next built an optical selection rule for the possible symmetry of the excited state $|m\rangle$ at any polarization direction (Table S2). For example, as shown in Figs. S5(a, b), the symmetry of a given initial state $|i\rangle$ and excited state $|m\rangle$ are A_g and B_{3u}, respectively. The photon polarization that connects these two symmetries has to be the B_{3u} representation, which corresponds to x-polarized light. For another transition (Fig. S5a, c), for instance B_{3u} to B_{1g}, the light polarization connecting these two symmetries with the B_{2u} representation has to be y-polarized.

Table S1: Character table for the D$_{2h}$ point group. Bulk PdPS belongs to the group D_{2h}^{14}, and the corresponding point group at the Γ point is D_{2h}.

D$_{2h}$	E	C$_2$	C$_2'$	C$_2''$	i	σ$_h$	σ$_v$	σ$_d$	Basis
A$_g$	1	1	1	1	1	1	1	1	x^2, y^2, z^2
B$_{1g}$	1	1	-1	-1	1	1	-1	-1	xy
B$_{2g}$	1	-1	-1	1	1	-1	1	-1	xz
B$_{3g}$	1	-1	1	-1	1	-1	-1	1	yz
A$_u$	1	1	1	1	-1	-1	-1	-1	xyz
B$_{1u}$	1	1	-1	-1	-1	-1	1	1	z
B$_{2u}$	1	-1	-1	1	-1	1	1	-1	y
B$_{3u}$	1	-1	1	-1	-1	1	1	-1	x

[1]The D_{2h} point group possesses 8 irreducible representations.

[2]The D$_{2h}$ group has three nonequivalent C$_2$ axes. The one labelled "C$_2$" is the principal axis (z in canonical orientation). The other two are perpendicular to the principal axis: the C$_2'$ is the x axis and C$_2''$ the y axis.

[3]The D$_{2h}$ group possesses three nonequivalent mirror planes. The one labelled σ$_h$ is orthogonal to the principal C$_2$ axis and thus corresponds to the xy plane. The other two contain the principal axis: the σ$_v$ is the xz plane and the σ$_d$ the yz plane.

Table S2: Selection rules for optical transitions from an initial state $|i\rangle$ to an excited state $|m\rangle$ at the light polarization along x or y directions.

x		y	
$|i\rangle$	$|m\rangle$	$|i\rangle$	$|m\rangle$
A$_g$	B$_{3u}$	A$_g$	B$_{2u}$
B$_{1g}$	B$_{2u}$	B$_{1g}$	B$_{3u}$
B$_{2g}$	B$_{1u}$	B$_{2g}$	A$_u$
B$_{3g}$	A$_u$	B$_{3g}$	B$_{1u}$
A$_u$	B$_{3g}$	A$_u$	B$_{2g}$
B$_{1u}$	B$_{2g}$	B$_{1u}$	B$_{3g}$
B$_{2u}$	B$_{1g}$	B$_{2u}$	A$_g$
B$_{3u}$	A$_g$	B$_{3u}$	B$_{1g}$

Raman scattering process includes three steps: 1) By electron-photon interaction, photon absorption and electron excitation from an initial state $|i\rangle$ to an excited state $|m\rangle$; 2) By electron-phonon interaction, a conversion from the state $|m\rangle$ to $|m'\rangle$; 3) photon radiation by electron-photon interaction and an electron transition from the state $|m'\rangle$ to the initial state $|i\rangle$. Depending on the incoming and outgoing polarization, we can excite two kinds of phonon symmetries: (1) the A_g phonon modes for the xx- and yy-polarizations; (2) the B$_{2g}$ phonon mode for the xy- or yx-polarization. If the incoming and outgoing polarizations are parallel (not parallel) to each other, the

symmetry of $|m\rangle$ and $|m'\rangle$ should be equal (different). The selection rules for $|m\rangle$ and $|m'\rangle$ for a given initial state $|i\rangle$ and for the two given polarization directions are summarized in Tables S3 and S4.

Suppose that the initial state possesses the B_{3u} symmetry and two intermediate states $|m\rangle = |m'\rangle = B_{1g}$ by the selection rules, the corresponding phonon mode that can be excited is the A_g phonon modes. For example, if the intermediate states are the A_g representations, the transition will be allowed for the B_{3u} initial state with yy-polarization (see Table S3). For the allowed transition of the B_{2g} phonon mode, $|m\rangle$ and $|m'\rangle$ have different symmetries. For example, the initial state has A_g symmetry, and the two intermediate states have B_{3u} and B_{2u} symmetry. According to the equ. S(10)[1], the transition will be allowed for the A_g initial state with xy-polarization (see Table S4), and the shape of the polar plot is the product of the shapes in Figure S5(e).

Therefore, depending on the band symmetry, we can understand the polarization dependences (i.e., linear dichroism transition) for the absorption and Raman spectra.

Table S3: Selection rules for intermediate states $|m\rangle$ and $|m'\rangle$ for a given initial state $|i\rangle$, and for polarization vector xx or yy, which correspond to the A_g phonon excitation. The selection rules correspond to the following product of matrix elements: $\langle f | H_{op} | m'\rangle\langle m' | H_{ep}(A_g) | m\rangle\langle m | H_{op} | i\rangle$ with $\langle f | = \langle i |$.

	xx		yy	
$|i\rangle$	$|m\rangle = |m'\rangle$	$|i\rangle$	$|m\rangle = |m'\rangle$
A_g	B_{3u}	A_g	B_{2u}
B_{1g}	B_{2u}	B_{1g}	B_{3u}
B_{2g}	B_{1u}	B_{2g}	A_u
B_{3g}	A_u	B_{3g}	B_{1u}
A_u	B_{3g}	A_u	B_{2g}
B_{1u}	B_{2g}	B_{1u}	B_{3g}
B_{2u}	B_{1g}	B_{2u}	A_g
B_{3u}	A_g	B_{3u}	B_{1g}

Table S4: Selection rules for intermediate states m and m' for a given initial state $|i\rangle$, and for polarization vector xy or yx which both correspond to the B_{2g} phonon

excitation. The selection rules correspond to the following product of matrix elements:

$$\langle f | H_{op} | m' \rangle \langle m' | H_{ep}(B_{2g}) | m \rangle \langle m | H_{op} | i \rangle \text{ with } \langle f | = \langle i |.$$

	xy			yx	
$|i\rangle$	$|m\rangle$	$|m'\rangle$	$|i\rangle$	$|m\rangle$	$|m'\rangle$
A_g	B_{3u}	B_{2u}	A_g	B_{2u}	B_{3u}
B_{1g}	B_{2u}	B_{3u}	B_{1g}	B_{3u}	B_{2u}
B_{2g}	B_{1u}	A_u	B_{2g}	A_u	B_{1u}
B_{3g}	A_u	B_{1u}	B_{3g}	B_{1u}	A_u
A_u	B_{3g}	B_{2g}	A_u	B_{2g}	B_{3g}
B_{1u}	B_{2g}	B_{3g}	B_{1u}	B_{3g}	B_{2g}
B_{2u}	B_{1g}	A_g	B_{2u}	A_g	B_{1g}
B_{3u}	A_g	B_{1g}	B_{3u}	B_{1g}	A_g
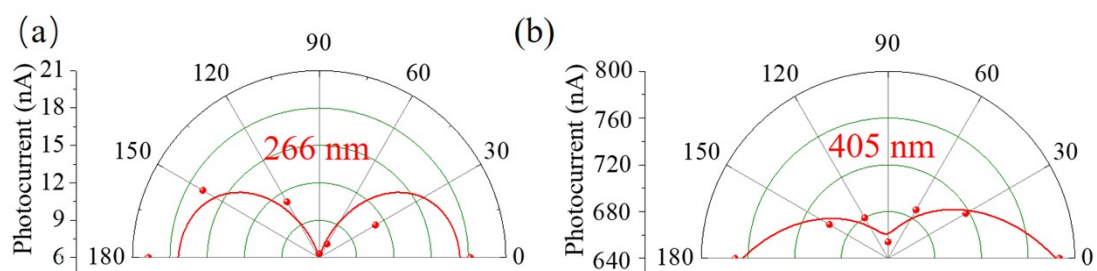
Fig S6. (a) Angle-dependent photocurrents under the 266 nm. (b) Angle-dependent photocurrents under the 405 nm.
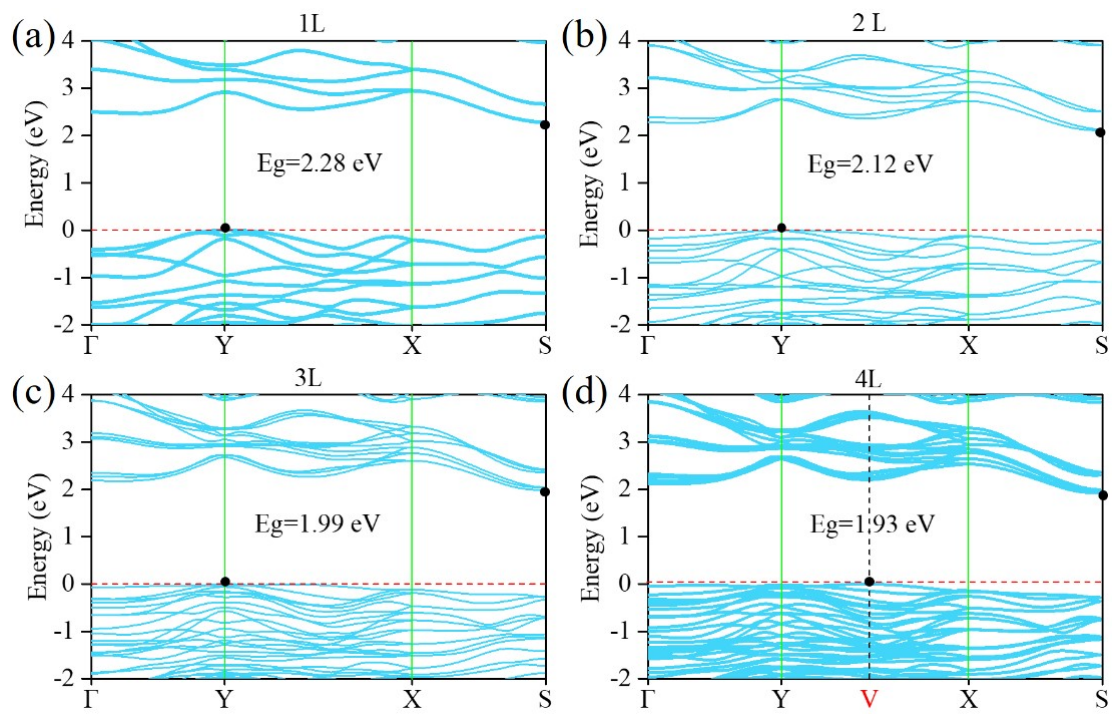
Fig S7. Electronic band structures of few-layer PdPS calculated with the HSE06 functional. Electronic band structures of 1L (a), 2L (b), 3L (c) and 4L (d). The valence band maximum (VBM) and conduction band minimum (CBM) are highlighted by solid black ball.
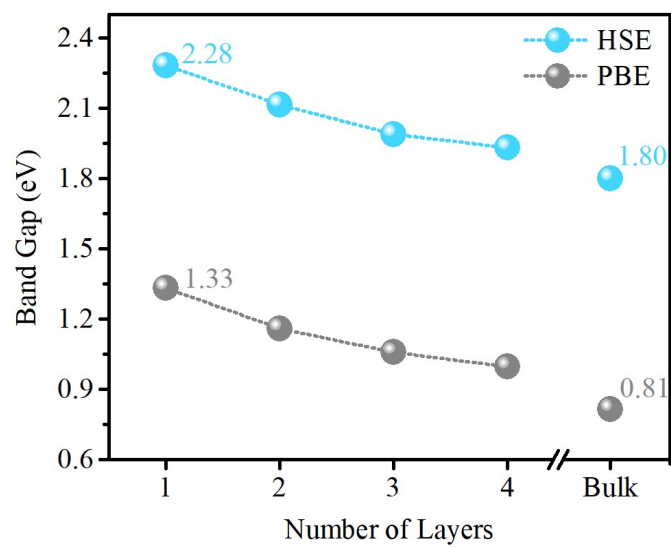
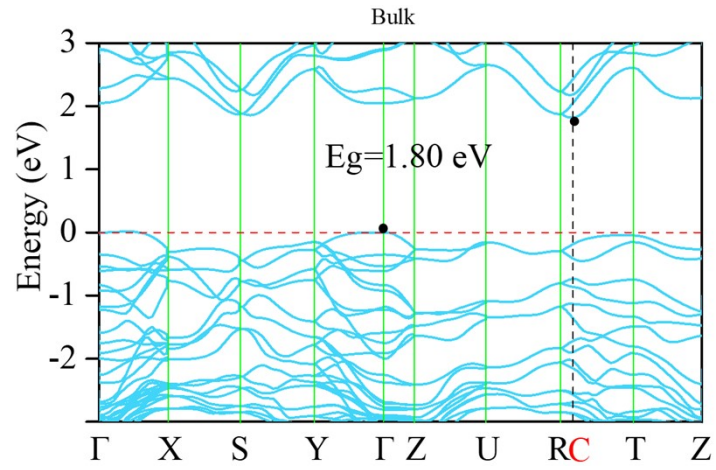**Fig S8.** Calculated band gap as a function of the number of layers through the HSE06 and PBE functionals.

Fig S9. Electronic band structure of bulk PdPS calculated with the HSE functional. Unlike few-layer PdPS, the VBM of the bulk phase locates Γ point, and the CBM is at the C point along R-T path.
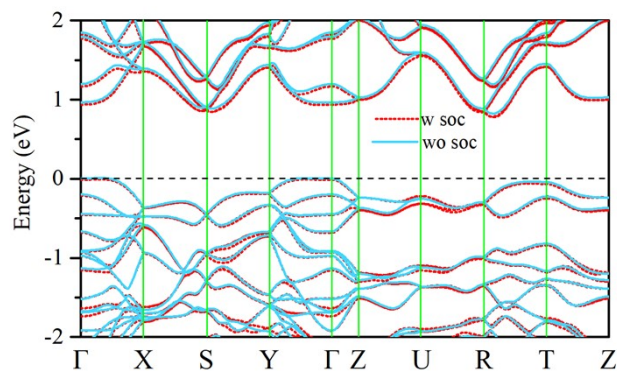
Fig S10. Electronic band structures for bulk PdPS with consideration of spin-orbit coupling (red dash line) and without consideration of spin-orbit coupling (cyan solid line). The calculation is carried out by PBE functional due to a low computational cost, which does not change the conclusion of this work by the HSE06 method.

We calculated and compared the band diagrams using the PBE method with/without consideration of the spin-orbit coupling (SOC) effect, as shown in Figure S10. The result indicates that the effect of spin-orbit coupling on the band character is relatively weak near the Fermi level. The splitting for somewhere in band structure is the consequence of both structural symmetry and spin-orbit coupling effect, such as splitting at the valence band at U point.
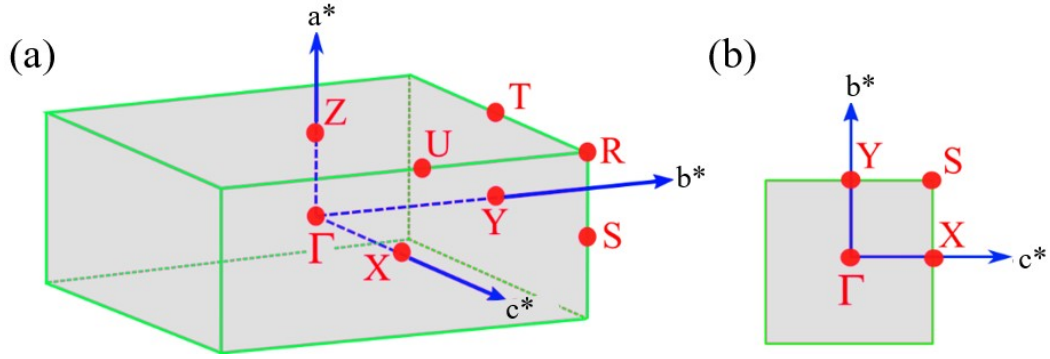
Fig S11. The first Brillouin Zone of the primitive cell for the bulk PdPS (left) and for the 2D PdPS (right). High-symmetric k points and paths are shown.

Computational methods:

The projector-augmented-wave method [2] with a plane-wave basis set implemented in the Vienna Ab initio Simulation Packages [3] was performed for the DFT calculations. The DFT-D2 method [4] was adopted for describing the vdW interaction. For all calculations, the energy cut-off for the wavefunction was 400 eV. The k-point girds mesh of $9 \times 9 \times 5$ and 9×9 are taken for the 3D and 2D fist Brillouin zone, respectively. The total energy of the systems was converged to 10^{-5} eV, and the force convergence criterion was set to 0.02 eV Å^{-1}. The electronic properties calculations (band structure and optical absorption spectra) were carried out by hybrid functional of Heyd, Scuseria, and Emzerhof (HSE06) [5] based on the optimized geometries. More details for calculating the optical absorption spectra can be referred to in previous literatures. [1, 6] The lattice parameters of bulk PdPS are fully optimized, yielding $b = 5.697$ Å, $c = 5.671$ Å, and $a = 13.317$ Å, in consistence with the experimental data ($b = 5.693$ Å, $c = 5.678$ Å, and $a = 13.304$ Å) [7], and the theoretical results ($b = 5.693$ Å, $c = 5.678$ Å, and $a = 13.304$ Å) [8]. In comparison, the optimized lattice constants of few layers are summarized in Table S5.

Table S5: Lattice constants of N-layer PdPS with the DFT-D2 vdW correction.

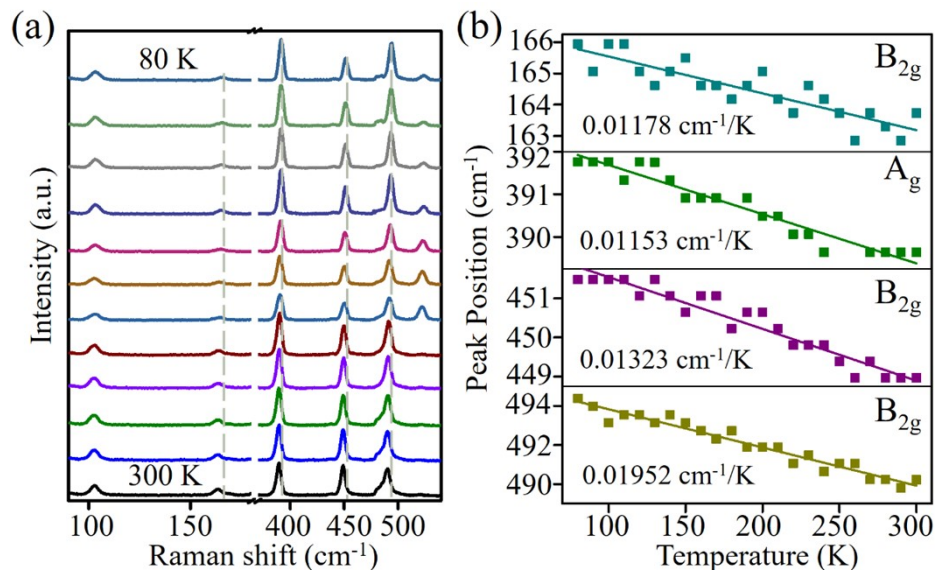|	b	c
1L	5.687	5.636
2L	5.690	5.654
3L	5.691	5.656
4L	5.695	5.664

Fig S12. Raman spectroscopy of 2D PdPS. (a) Raman spectra of the PdPS flake measured in the temperature range from 80 to 300 K. (b) Temperature dependence of the Raman peak positions of B_{2g} and A_g modes.
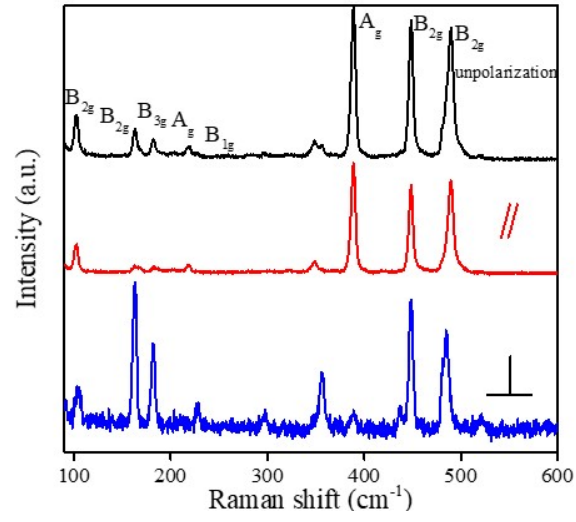
Fig S13. Normalized Raman spectra measured at angle of $0°$ under un-, parallel-, and cross-polarized configurations.
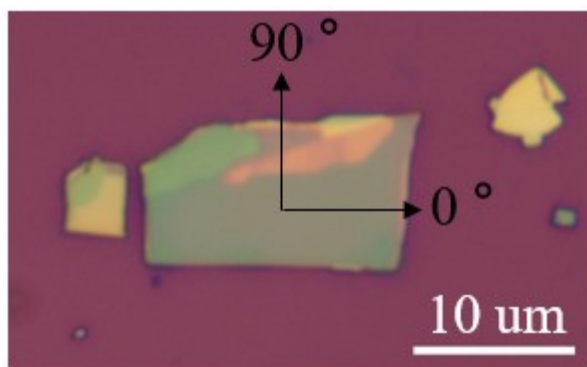
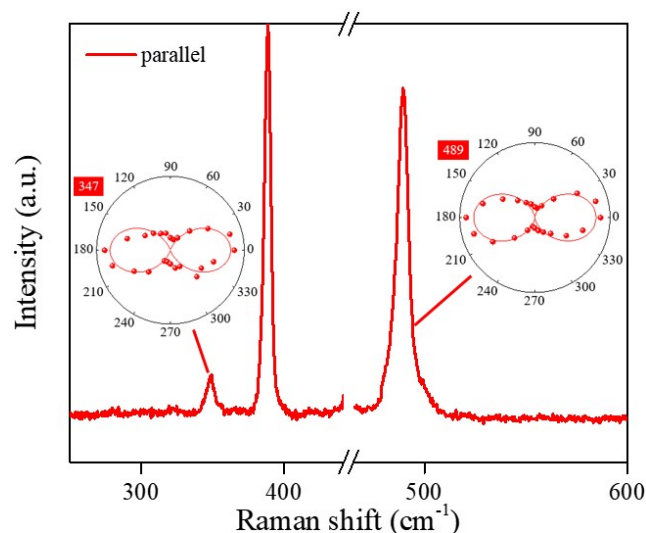**Fig S14.** Typical OM image of exfoliated PdPS flake.

Fig S15. ARPRS results under the parallel polarization configuration. Polar plot and fitting of 347 cm^{-1} and 489 cm^{-1} modes. The inset show experimental (red dots) and fitted (red curves) polar plots of the peak intensities versus rotation angle.

Supplementary References

1 L. Li, P. Gong, D. Sheng, S. Wang, W. Wang, X. Zhu, X. Shi, F. Wang, W. Han, S. Yang, K. Liu, H. Li and T. Zhai, *Adv. Mater.*, 2018, **30**, 1804541.

2 P. E. Blochl, *Phys. Rev. B*, 1994, **50**, 17953-17979.

3 J. Hafner, *J Comput Chem*, 2008, **29**, 2044-2078.

4 S. Grimme, *J Comput Chem*, 2006, **27**, 1787-1799.

5 J. Heyd and G. E. Scuseria, *J. Chem. Phys.*, 2004, **120**, 8208-8215.

6 P. L. Gong, F. Zhang, L. Li, B. Deng, H. Pan, L. F. Huang and X. Q. Shi, *J. Phys. Condens. Matter.*, 2019, **31**, 395501.

7 W. JEITSCHKO, *Acta Cryst.*, 1974, 2565.

8 S. N. Gupta, A. Singh, S. Sarkar, D. V. S. Muthu, S. Sampath, U. Waghmare and A. K. Sood, *Phys. Rev. B*, 2020, **101**, 035123.